Danmarks Tekniske Universitet

DTU

Assignment # 2
Turbulent flows

Authors

[redacted]

Szczepan Zygmunt Letkiewicz - s244067

November 18, 2024

Contents

1 Introduction

This report explores the behaviour of wave boundary layers under varying flow conditions and surface characteristics. This is achieved through the use of a RANS $k-\omega$ turbulence model developed by Fuhrman et. al. [1], and is further supported through the use of experimental data collected by Jensen et. al. [2]. This investigation begins with estimates of flow resistance and considerations for near-wall grid spacing to capture boundary interactions accurately. Four main cases are examined: laminar, transitional, and turbulent wave boundary layers, with the latter assessed over both smooth and rough beds. By comparing these cases, we explore how surface roughness impacts flow resistance, mean velocity, and turbulence. The findings provide insights into wave-boundary interactions crucial for applications in coastal and engineering contexts.

2 Flow Resistance Estimates

Prior to running the simulations for the different turbulence modelling cases, it is possible to predict some of their characteristic properties. For instance, the wave friction factor f_w can be calculated differently across flow regimes to estimate flow resistance for each case. Based on the equations in [3], these calculations can be summarized as follows:

1. **Laminar boundary layer**: For cases where the bed is smooth and $Re \leq 1.5 \times 10^5$, indicative of laminar flow, f_w is determined using Equation 5.59 in [3]:

$$f_w = \frac{2}{\sqrt{Re}} \tag{1}$$

2. **Transitional wave boundary layer**: Note that for wave boundary layers which fall in the transitional regime, it is difficult to accurately predict the wave friction factor due to the rapidly changing behavior of the flow. Therefore, to avoid underestimating f_w, a conservative approach should be used: the equation yielding the higher f_w value based on the flow's Reynolds number, whether from Equation 1 or Equation 2, should be selected.

3. **Smooth bed, turbulent wave boundary layer**: For cases where the bed is smooth and $Re \geq 5 \times 10^5$, typical of fully turbulent flow boundary layers, f_w is computed using Equation 5.60 in [3]:

$$f_w = \frac{0.035}{Re^{0.16}} \tag{2}$$

4. **Rough bed, turbulent wave boundary layer**: For turbulent wave boundary layer cases with rough beds, the friction coefficient is calculated using Equation 5.69 in [3]:

$$f_w = \exp\left[5.5 \cdot \left(\frac{a}{k_s}\right)^{-0.16} - 6.7\right] \tag{3}$$

Furthermore, the maximum bed friction velocity U_{fm} can also be calculated based on the estimates for f_w and the free stream velocity magnitude U_{0m} for the different flow cases. U_{fm} relates the shear stress generated at the bed boundary with the free stream velocity and can be calculated using Equation 4:

$$U_{fm} = \sqrt{\frac{f_w}{2}} \cdot U_{0m} \tag{4}$$

The results of this analysis are presented in Table 1.

3 Near Wall Grid Spacing

The viscous sublayer will develop regardless of the near wall type, requiring an adequate cell size Δy to model the flow. [3] suggests that the grid spacing should be sufficiently small to satisfy the following conditions in Equation 5.

$$\Delta y^+ = \frac{\Delta y U_f}{\nu} \leq 1 \tag{5}$$

This criterion will ensure that a sufficient number of cells will be located in the viscous sublayer region. The following rule of thumb in Equation 6, is implemented to determine the cell size.

$$\frac{\Delta y}{k_s} \leq 0.02 \tag{6}$$

The parameter k_s in Equation 6 is the surface roughness, which can be also expressed in its dimensionless form k_s^+ shown in Equation 7.

$$k_s^+ = \frac{k_s U_f}{\nu} \tag{7}$$

The dimensionless form is used to depict the flow regime where $k_s^+ \leq 5$ is considered hydraulically smooth, and $k_s^+ \geq 70$ is hydraulically rough. To obey this rule, a k_s^+ of 0.1 is selected for smooth-walled cases 1-3 to determine the surface roughness k_s. On the other hand, the given surface roughness $k_s = 0.00084$ m for the rough walled case 4, is used to determine the corresponding k_s^+. This value is calculated to be 76.52, indicating that the surface is sufficiently rough to yield a hydraulically rough regime.

Table 1: Results of numerical analysis for each case.

Case nr.	f_w	U_{fm} [m/s]	Δy [m]	k_s [m]	k_s^+
1	0.007454	0.01404	8.12×10^{-5}	8.11×10^{-6}	0.10
2	0.004132	0.03091	3.69×10^{-5}	3.69×10^{-6}	0.10
3	0.002930	0.07655	1.49×10^{-5}	1.49×10^{-6}	0.10
4	0.005392	0.10385	1.68×10^{-5}	0.00084	76.52

4 Case 1: Laminar Wave Boundary Layer

For the first simulation, the flow has a Reynolds number of $Re = 7.2 \cdot 10^4$, corresponding to the laminar flow regime. Figure 1 plots two laminar velocity profiles, one following the laminar theory and the other using a RANS $k - \omega$ simulation. The profiles are plotted at four distinct time instances based on the wave angular frequency, ranging from $0 - 135°$. Note that the vertical axis has been non-dimensionalised by dividing by the amplitude of the orbital motion of water particles just outside the boundary layer a. Similarly, the horizontal axis has been non-dimensionalised by dividing by the free stream velocity magnitude U_{0m}.

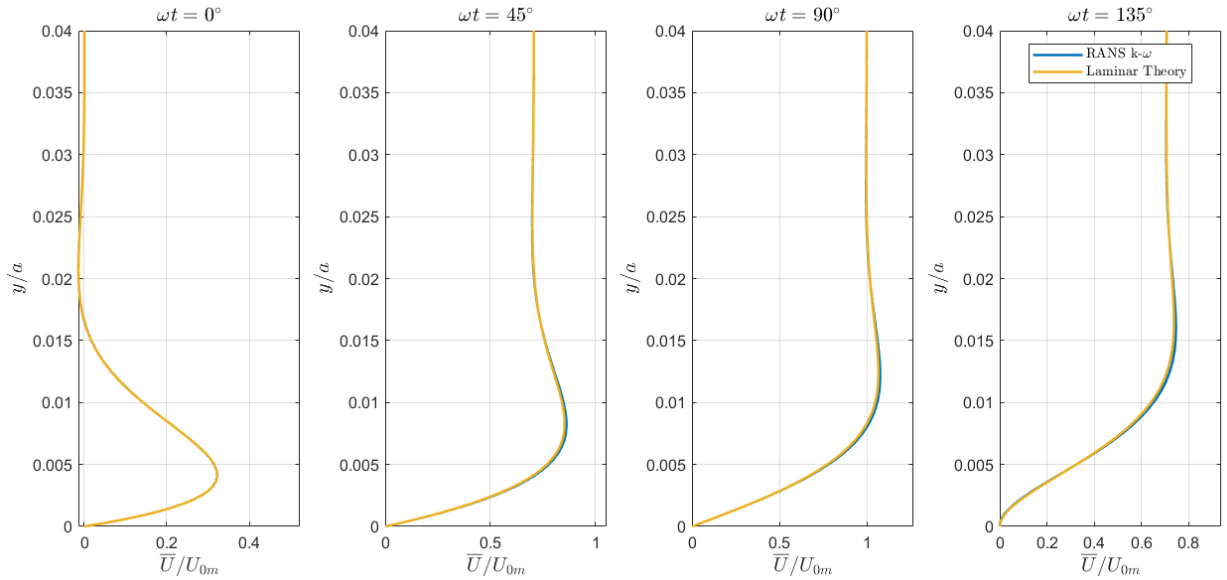

Figure 1: Time development of velocity profiles in laminar wave boundary for phases $\omega t = 0°, 45°, 90°$ and $130°$. Comparison of RANS $k - \omega$ model with laminar solution.

Several conclusions can be made from Figure 1. Firstly, it is clear that the flow near the bed leads over the flow in the free stream region. As a result, any changes in the boundary layer due to pressure gradient variations will be felt by the near-bed flow first, as the shear stresses created by the bed-flow interaction allow for a quicker dissipation of momentum. This may also explain the overshooting behaviour of the velocity profiles, which at first display a flow velocity higher than the free stream velocity. Furthermore, it can also be concluded that in the laminar case, the laminar theory aligns almost perfectly with the RANS simulation results. This suggests that the assumptions and simplifications which were made to develop this theory are valid for the case in question.

Figure 2 plots the variation of the bed shear stress over a full cycle.

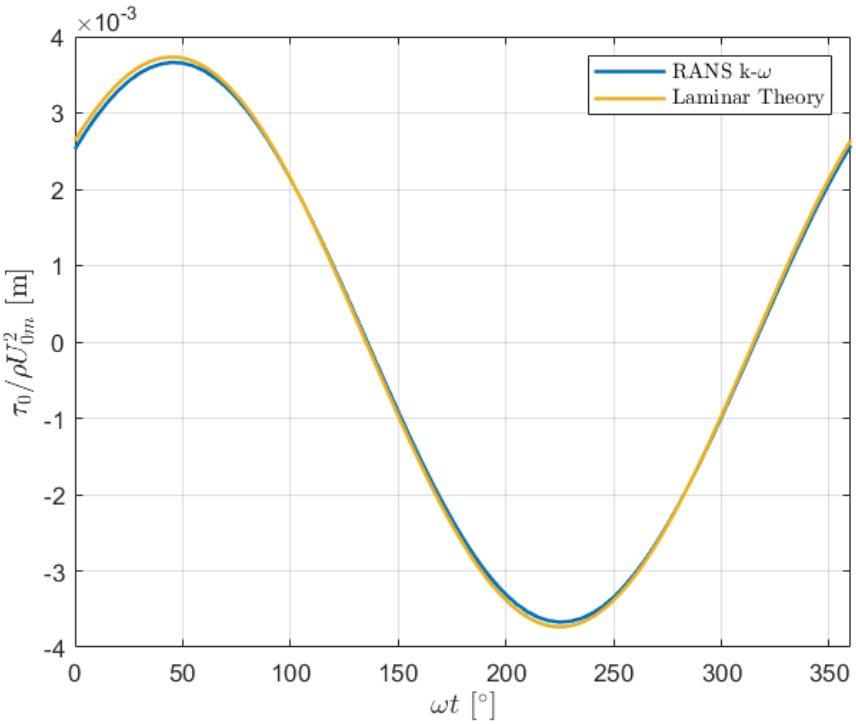

Figure 2: Time series of bed shear stress for case 1, comparing RANS $k-\omega$ model [3] with laminar solution.

Figure 2 shows how the bed shear stress follows a sinusoidal pattern, in accordance with the oscillatory motion of the water just outside of the boundary layer U_0, where $U_0 = U_{0m}\sin(\omega t)$. However, the plot also shows how the bed shear stress leads over the free stream flow by a phase lead of approximately 45°. This means that the flow will reverse 45° earlier at the bed than outside the laminar wave boundary layer. Lastly, once again the laminar theory and RANS simulation output nearly identical results.

5 Case 2: Transition Wave Boundary Layer

Case 2 deals with the wave boundary layer in the transition regime, at a Reynolds number $Re = 6.3 \cdot 10^5$. Figure 3 plots the bed shear stress calculated from laminar theory, the RANS $k - \omega$ model output and some experimental data for the beginning of the cycle.

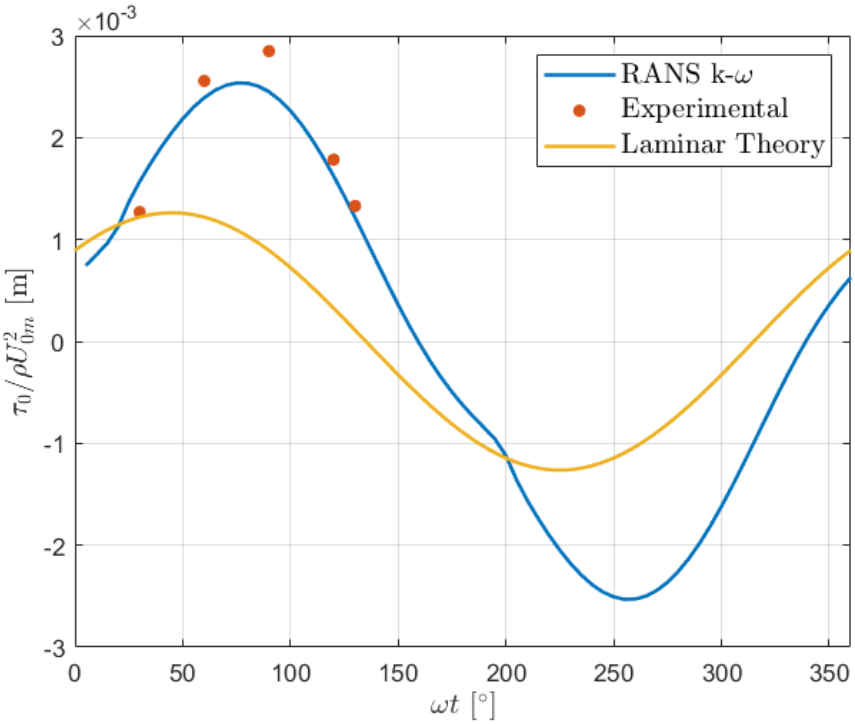

Figure 3: Time series of bed shear stress for case 2 comparing experimental data from [2], RANS $k - \omega$ [3] model with laminar solution.

In contrast with case 1, the bed shear stress plot now shows a very big disparity between the laminar theory and RANS $k - \omega$ model, with the laminar theory underpredicting the shear stress values for the majority of the wave period. This is because the laminar theory fails to predict the turbulence effects being generated at the bed due to an increase in Re. The RANS simulation output seems to resemble the experimental data to a higher degree, although there are still some noticeable differences due to the dual laminar and turbulent nature of the transition region.

Furthermore, it is now also possible to plot the normalized friction coefficient f_w^* as a function of the phase range, as shown in Figure 4.

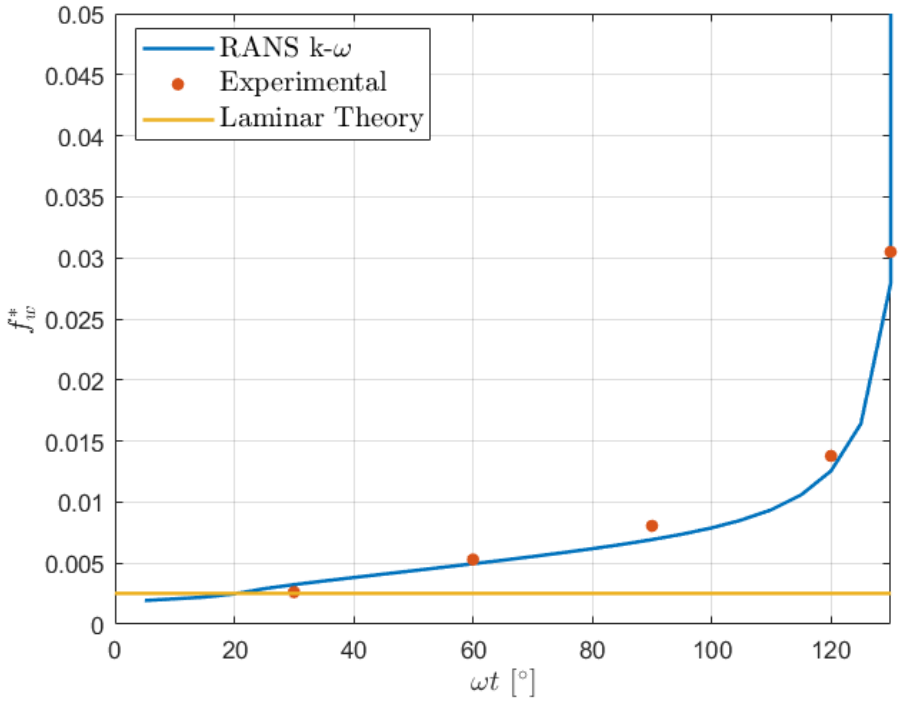

Figure 4: Time evolution of normalized friction coefficient for phase range of $0° \leq \omega t \leq 130°$ comparing experimental data from [2] with RANS $k - \omega$ model [3].

This plot further illustrates the limitations of laminar theory in the transition region. Laminar theory predicts that the normalized friction coefficient remains constant at 0.0025 throughout the entire phase range, whereas in reality both the experimental data and RANS simulation show an exponential increase as ωt approaches 130°. Considering the values of the friction factor f_w in section 2, the more conservative choice of estimating f_w as turbulent is seen to be more promising. Figure 3 and Figure 4 both show that laminar theory begins to deviate from reality at approximately 30°, marking the start of the laminar-to-turbulent transition of the boundary layer. This behaviour seems to agree with the results presented in Figure 5.17 in [3], which predicts this transition at a similar phase for the Reynolds number at hand.

6 Case 3: Turbulent, Smooth-bed Wave Boundary Layer

Case 3 features a Reynolds number $Re = 5.4 \cdot 10^6$, which corresponds to a turbulent wave boundary layer. The velocity profile for this case is plotted in Figure 5 for a number of time phases, as well as Reynold's stresses as shown in Figure 6.

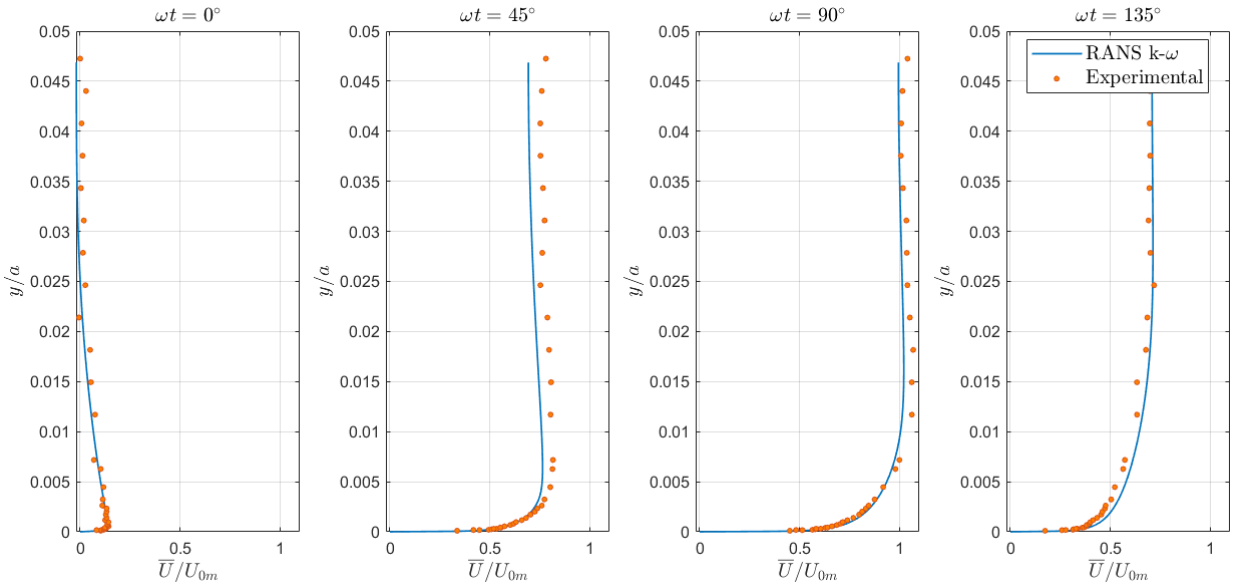

Figure 5: Time development of velocity profiles in a smooth-bed, turbulent wave boundary for phases $\omega t = 0°, 45°, 90°$ and $130°$. Comparison of RANS $k - \omega$ model with experimental data.

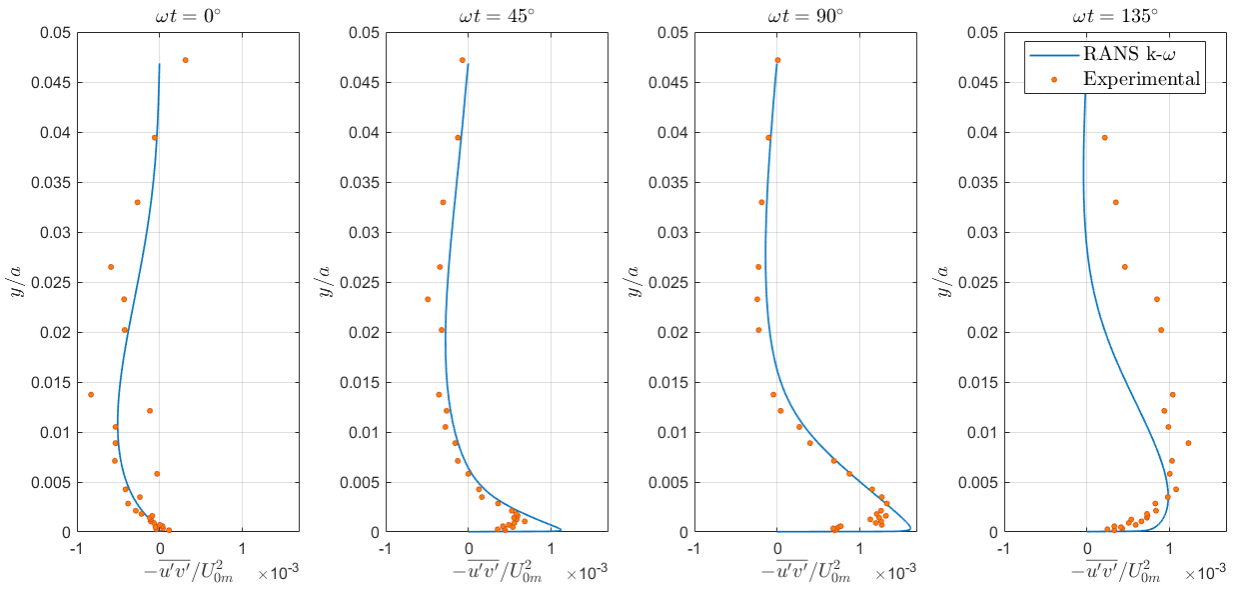

Figure 6: Time development of Reynolds stresses in a smooth-bed, turbulent wave boundary for phases $\omega t = 0°, 45°, 90°$ and $130°$. Comparison of RANS $k - \omega$ model with experimental data.

Firstly, Figure 5 shows how the velocity profile follows a similar behaviour to that of the laminar case, with the flow near the bed leading over the flow in the free stream region.

However, in this case, the overshooting of the velocity is much less noticeable as the turbulent behaviour of the flow facilitates quicker momentum transfer. Furthermore, Figure 6 shows how the turbulence builds up near the bed during the first phases. As the boundary layer develops in time, the turbulence diffuses and becomes more uniformly distributed along the height.

Based on the turbulent components, it is also possible to plot the kinetic energy of the flow as shown in Figure 7. Once again, this follows a comparable pattern to that of the Reynolds stresses, with the region close to the bed experiencing higher kinetic energy which is then diffused at higher points in the boundary layer. Note that here the RANS estimate for turbulent kinetic energy seems to underestimate the actual values when compared to the experimental results for all phases, but generally follows a similar pattern.

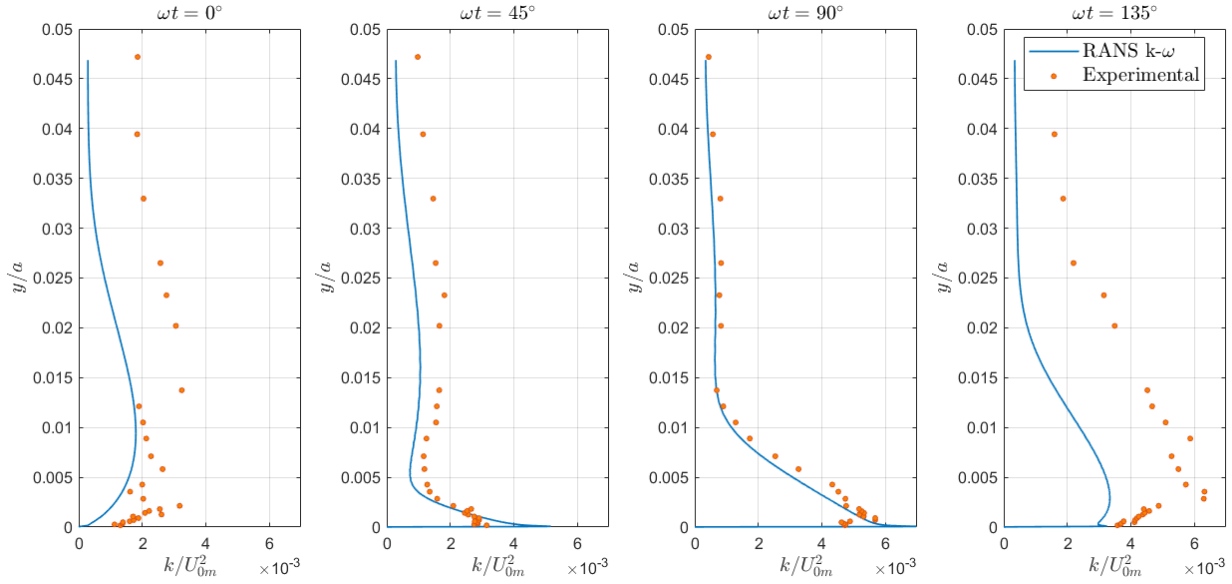

Figure 7: Time development of turbulent kinetic energy in a smooth-bed, turbulent wave boundary for phases $\omega t = 0°, 45°, 90°$ and $130°$. Comparison of RANS $k - \omega$ model with experimental data.

Lastly, the bed shear stress as a function of phase can also be plotted for this case, as shown in Figure 8. Similarly to the laminar case, the bed shear stress for the smooth-bed turbulent case follows a sinusoidal pattern. However, it is worth noting that now the phase lead of the bed shear stress with respect to the free stream flow is much lower than before for all phases. This indicates an almost immediate laminar-to-turbulent transition, as the turbulent nature of the flow, allows for quicker momentum transfer and thus reduces the phase lead very significantly. Based on the graph this is seen to occur at a phase ωt of approximately $5 - 15°$, where it starts deviating very considerably from laminar theory.

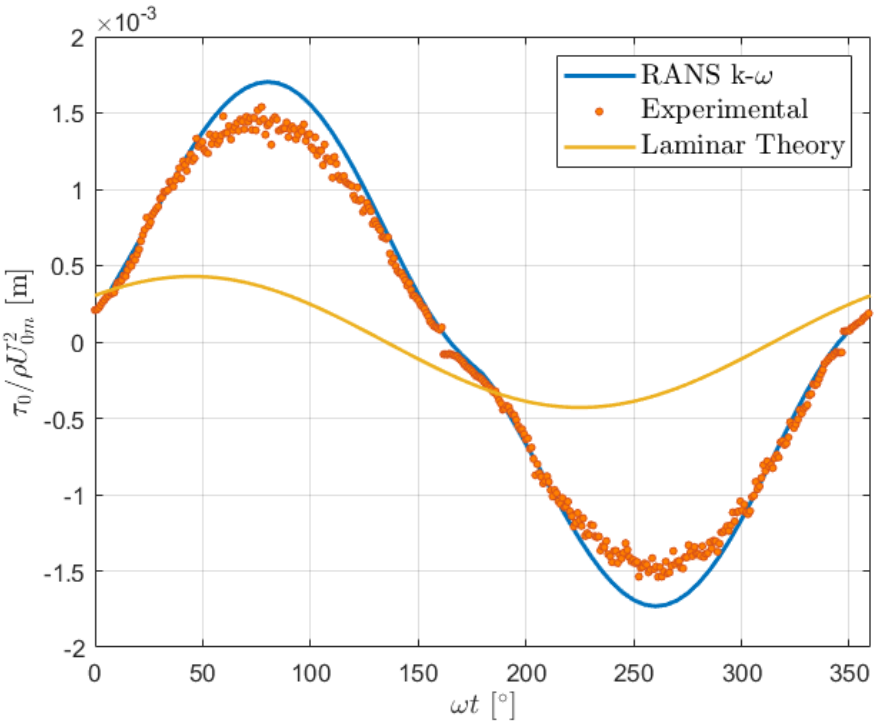

Figure 8: Time series of bed shear stress for case 3 comparing experimental data from [2] and RANS $k-\omega$ [3].

7 Case 4: Turbulent, Rough-bed Wave Boundary Layer

For the last case, the smooth-bed present in case 3 is now replaced with a rough-bed, while the Reynolds number is kept the same. Following a similar approach to that in case 3, the same quantities can be plotted to make a comparison of the roughness effects on the wave boundary layer. These are presented in Figure 9 - Figure 12:

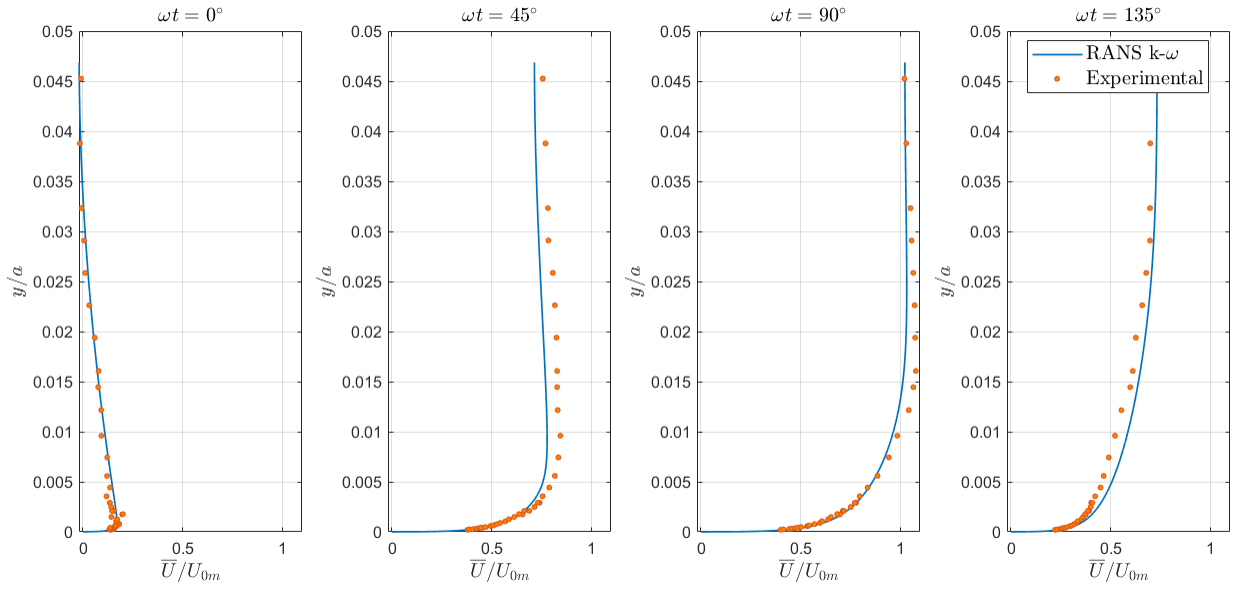

Figure 9: Time development of velocity profiles in a rough-bed, turbulent wave boundary for phases $\omega t = 0°, 45°, 90°$ and $130°$. Comparison of RANS $k - \omega$ model with experimental data.

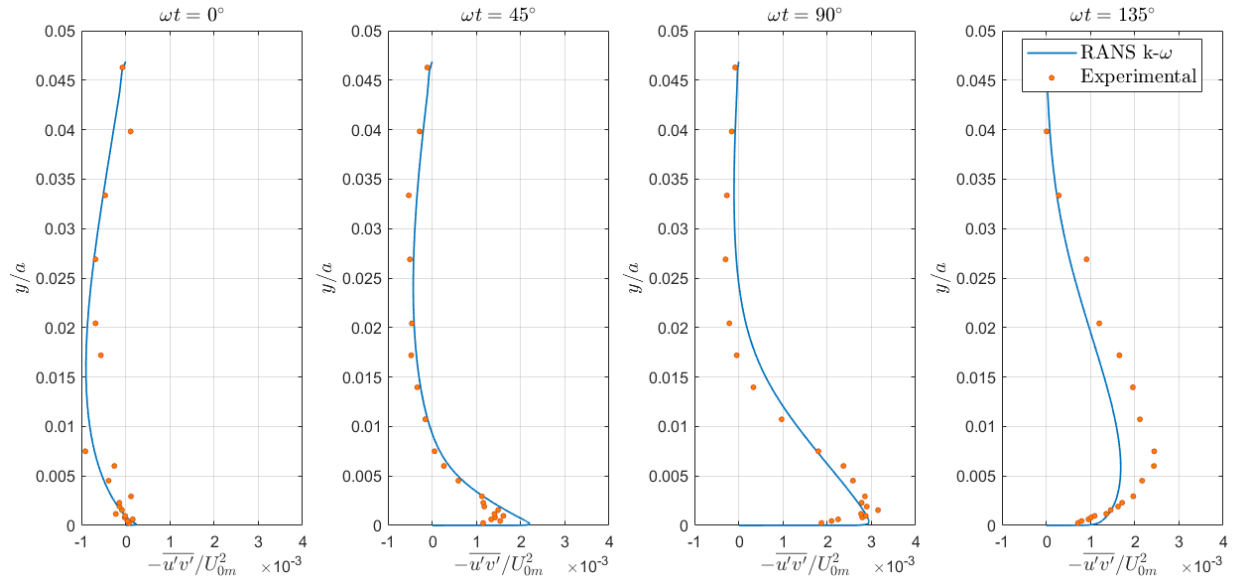

Figure 10: Time development of Reynolds stresses in a rough-bed, turbulent wave boundary for phases $\omega t = 0°, 45°, 90°$ and $130°$. Comparison of RANS $k - \omega$ model with experimental data.

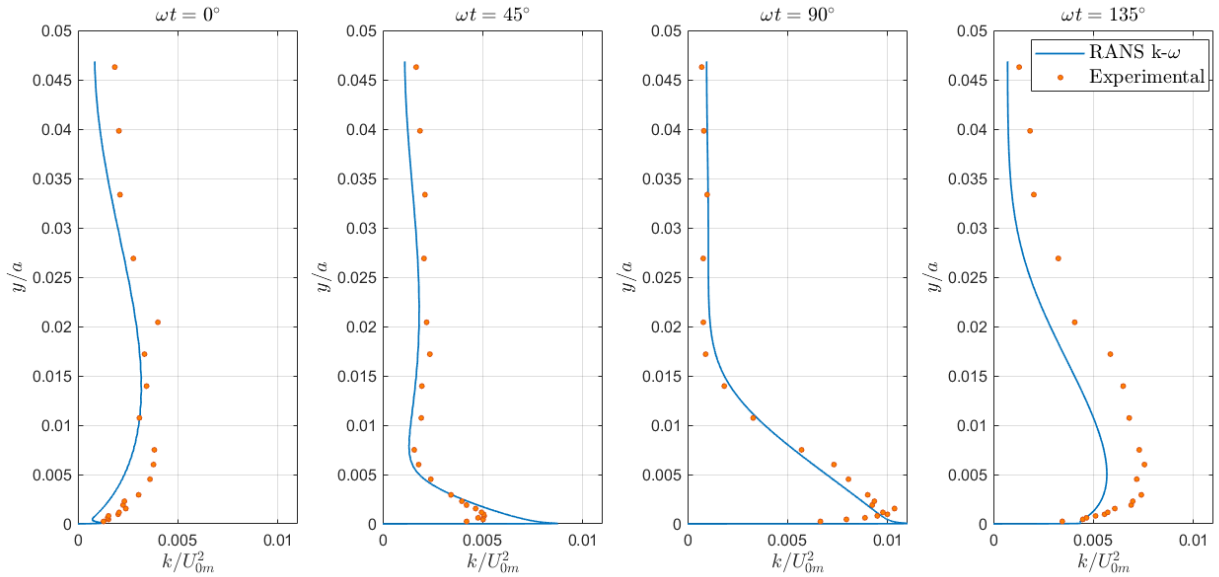

Figure 11: Time development of turbulent kinetic energy in a rough-bed, turbulent wave boundary for phases $\omega t = 0°, 45°, 90°$ and $130°$. Comparison of RANS $k - \omega$ model with experimental data.

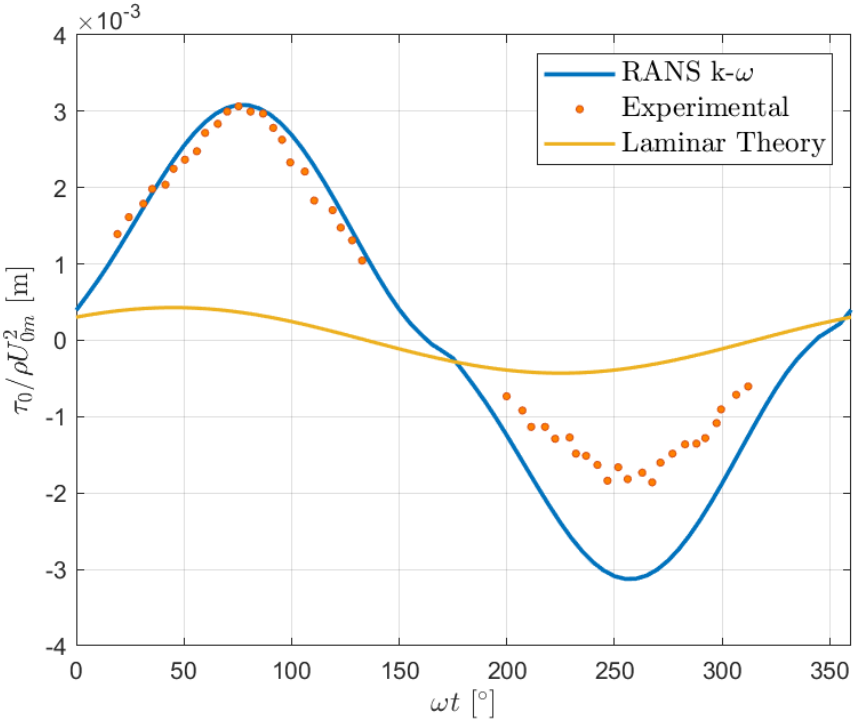

Figure 12: Time series of bed shear stress for case 4 comparing experimental data from [2] and RANS $k - \omega$ [3].

A number of conclusions can be made from these plots. Firstly, the flow and turbulence behaviour over a rough bed during one half-cycle seems to be qualitatively similar to smooth-bed flows. However, adding roughness decreases the mean flow velocity slightly while increasing turbulence levels (and thus kinetic energy). This effect diminishes with distance from the bed until a point is reached where the mean flow velocity becomes similar for both smooth and rough cases. For turbulence quantities, the influence of roughness fades at a slightly greater distance. The decrease in mean velocity results from the rough boundary's resistance, whereas the rise in turbulence can be explained by enhanced momentum transfer caused by the roughness elements. Note that in terms of bed shear stress, for the rough-bed case, the results follow a similar pattern to the smooth case, however, the magnitude of the stresses is twice as large. These findings are further illustrated in a more clear, visual manner in Figure 13, which compares the smooth and rough bed cases at a phase of $\omega t = 90°$:

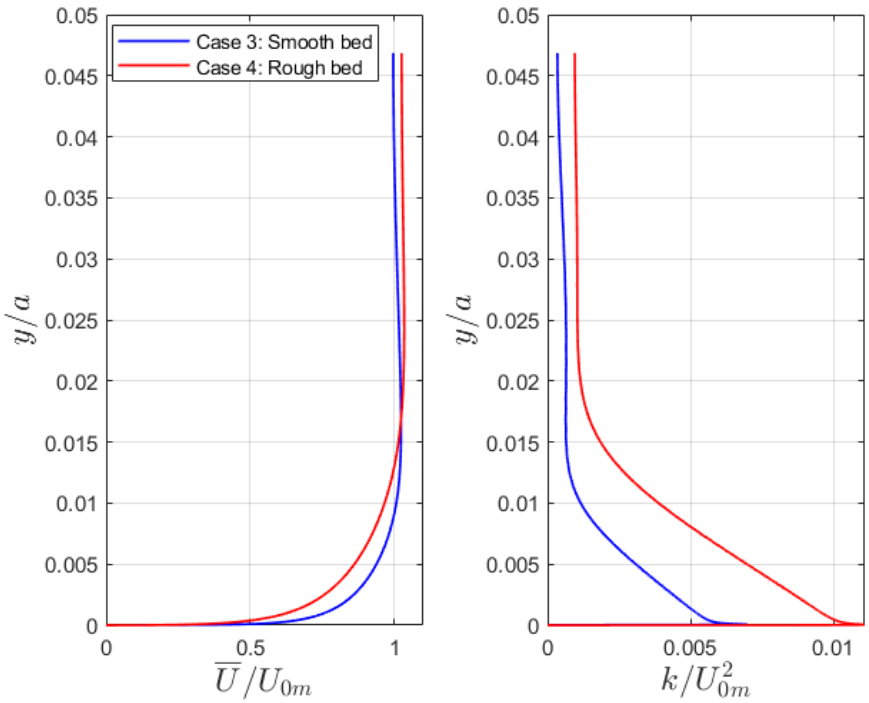

Figure 13: Comparison of computed velocity and turbulent kinetic energy profiles for smooth-bed and rough-bed turbulent wave boundary layer at phase $\omega t = 90°$.

8 Conclusion

In conclusion, this report provides a comprehensive analysis of wave boundary layers across different flow regimes. Examining the time development of velocity profile, Reynolds stress, and kinetic energy has shown the expected behaviour as well as the differences and difficulties of predicting the flow behaviour. The comparison of experimental data with the RANS $k - \omega$ model highlights these discrepancies for rough as well as smooth wall flow.

List of Figures

References

[1] D. Fuhrman, S. Schløer, and J. Sterner, "Rans-based simulation of turbulent wave boundary layer and sheet-flow sediment transport processes," *Coastal Engineering*, vol. 73, pp. 151–166, 2013.

[2] B. Jensen, B. Sumer, and J. Fredsoe, "Turbulent oscillatory boundary layers at high reynolds numbers," *Journal of Fluid Mechanics*, vol. 206, pp. 265 – 297, 09 1989.

[3] B. M. Sumer and D. R. Fuhrman, *Turbulence in Coastal and Civil Engineering*. Advanced Series on Ocean Engineering, World Scientific, 2020.